Correspondence

Robust Extended Kalman Filtering for Nonlinear Systems With Stochastic Uncertainties

Xiong Kai, Chunling Wei, and Liangdong Liu

***Abstract*—In this correspondence paper, a novel robust extended Kalman filter (REKF) for discrete-time nonlinear systems with stochastic uncertainties is proposed. The filter is derived to guarantee an optimized upper bound on the state estimation error covariance despite the model uncertainties as well as the linearization errors. Further analysis shows that the proposed filter has robustness against process noises, measurement noises, and model uncertainties. In addition, the new method is applied in an X-ray pulsar positioning system. It is illustrated through numerical simulations that the REKF is more effective than the standard extended Kalman filter and the extended robust H_∞ filter.**

***Index Terms*—Nonlinear estimation, nonlinear uncertain system, pulsar positioning system, robust extended Kalman filter (REKF).**

I. Introduction

During the last four decades, the Kalman filter and the extended Kalman filter (EKF) have been widely used for state estimation within communication and aerospace applications [1]–[3]. It is well known that the optimality of the Kalman filter holds only when the system model is accurate [4]. In most physical systems, the model uncertainties seriously degrade the filtering performance. Recently, robust H_∞ techniques have been introduced to cope with the uncertainties [5]–[7]. The design criterion of the H_∞ filter is to guarantee a bounded estimation error for bounded uncertainties. Robust Kalman filters for linear uncertain systems are studied in [8] and [9], and a robust H_∞ filter for nonlinear uncertain systems is proposed in [10]. This algorithm is obtained by solving a nonlinear Hamilton–Jacobi inequality. An extended robust H_∞ filter based on a linearization technique is established in [11] for nonlinear systems with an integral quadratic constraint uncertainty. The main advantage of the extended robust H_∞ filter is its simplicity, as no additional computing is required for the implementation of the algorithm (see [12] and [13] for other related works).

In this correspondence paper, a novel robust EKF (REKF) for nonlinear systems with stochastic uncertainties is proposed. The algorithm is designed to guarantee the finite upper bound on the estimation error and simultaneously minimize this upper bound. Our approach differs from the algorithm in [11], in that the key idea of the extended robust H_∞ filter is to insert extra terms with tuning parameters in the dynamic equation of the state estimate to compensate the model uncertainties, while the emphasis of the proposed algorithm is on the appropriate design of the filter gain so that the dependence of the state estimate on the information with the uncertainties will be mitigated. Note that the filtering performance is inevitably dependent upon how well the uncertainties of a practical system are reflected in the uncertainty model. Related to this issue, we give some explanations about how to establish the uncertainty model for the considered X-ray pulsar positioning system.

A pulsar positioning system is an autonomous navigation system for spacecrafts [14]–[16]. From 1999 to 2000, the U.S. Naval Research Laboratory's unconventional stellar aspect experiment onboard the Advanced Research and Global Observation Satellite was performed to demonstrate the feasibility of the pulsar-based navigation, and the positioning accuracies are on the order of 2 km. Generally, in order to establish the measurement model, the pulsar position should be measured. Due to the limitation of current technology, the accuracy of the pulsar position is rather low, and the inaccurate model parameters may degrade the positioning performance. In our prior work [17], the difference technique is adopted to eliminate the common error terms in the measurement model for satellites in constellations. In this correspondence paper, the robust filter is used to suppress the detrimental effects of the model uncertainties for a single spacecraft.

This correspondence paper is organized as follows. In Section II, the REKF is developed for nonlinear systems with stochastic uncertainties. The robust performance of the proposed algorithm is derived in Section III, and, in Section IV, we present an application of the REKF to the X-ray pulsar positioning system in comparison with the EKF and the extended robust H_∞ filter. Some conclusions are drawn in Section V.

II. Design of REKF

A. Problem Formulation

Consider the following nonlinear uncertain system:

$$\boldsymbol{x}_k = f(\boldsymbol{x}_{k-1}) + \boldsymbol{B}_k\eta_k\phi(\boldsymbol{x}_{k-1}) + \boldsymbol{w}_k \tag{1}$$

$$\boldsymbol{y}_k = h(\boldsymbol{x}_k) + \boldsymbol{D}_k\xi_k\psi(\boldsymbol{x}_k) + \boldsymbol{v}_k \tag{2}$$

where $\boldsymbol{x}_k \in R^l$ and $\boldsymbol{y}_k \in R^m$ denote the state and measurement vectors at time instant k, $f(\cdot)$ and $h(\cdot)$ are nonlinear functions that are assumed to be continuously differentiable, $\boldsymbol{B}_k \in R^{l\times l}$ and $\boldsymbol{D}_k \in R^{m\times l}$ are known time-varying matrices, and $\phi(\cdot)$ and $\psi(\cdot)$ are known nonlinear functions that satisfy

$$\mathrm{E}\left[\phi(\boldsymbol{x}_k)\phi^{\mathrm{T}}(\boldsymbol{x}_k)\right] \le \Xi_k \quad \mathrm{E}\left[\psi(\boldsymbol{x}_k)\psi^{\mathrm{T}}(\boldsymbol{x}_k)\right] \le \Theta_k \tag{3}$$

where $\Xi_k \in R^{l\times l}$ and $\Theta_k \in R^{l\times l}$ are known matrices. The inputs $\eta_k \in R$, $\xi_k \in R$, $\boldsymbol{w}_k \in R^l$, and $\boldsymbol{v}_k \in R^m$ are uncorrelated noises which have the following statistical properties:

$$\mathrm{E}(\eta_k) = 0 \quad \mathrm{E}(\xi_k) = 0 \quad \mathrm{E}(\boldsymbol{w}_k) = 0 \quad \mathrm{E}(\boldsymbol{v}_k) = 0 \tag{4}$$

$$\mathrm{E}\left\{\begin{bmatrix}\boldsymbol{w}_k\\ \boldsymbol{v}_k\\ \eta_k\\ \xi_k\end{bmatrix}\left[\boldsymbol{w}_j^{\mathrm{T}} \quad \boldsymbol{v}_j^{\mathrm{T}} \quad \eta_j \quad \xi_j\right]\right\} = \begin{bmatrix}\boldsymbol{Q}_k\delta_{kj} & & & \\ & \boldsymbol{R}_k\delta_{kj} & & \\ & & q_k\delta_{kj} & \\ & & & r_k\delta_{kj}\end{bmatrix} \tag{5}$$

Manuscript received April 25, 2007; revised October 9, 2008. First published November 13, 2009; current version published February 18, 2010. This work was supported in part by the National Natural Science Foundation of China under Grant 60702019, by the National High-Tech Research and Development Program of China under Grants 2007AA12Z325 and 2008AA12A203, and by the Basic Research Program of Deference Technology under Grant A0320080019. This paper was recommended by Associate Editor L. Fang.

The authors are with the National Laboratory of Space Intelligent Control, Beijing Institute of Control Engineering, Beijing 100080, China (e-mail: tobelove2001@tom.com).

Color versions of one or more of the figures in this paper are available online at http://ieeexplore.ieee.org.

Digital Object Identifier 10.1109/TSMCA.2009.2034836

where

$$q_k \leq 1 \quad r_k \leq 1 \tag{6}$$

and δ_{kj} denotes the Kronecker delta function. The terms $\boldsymbol{B}_k \eta_k \phi(\boldsymbol{x}_{k-1})$ and $\boldsymbol{D}_k \xi_k \psi(\boldsymbol{x}_k)$ represent the stochastic uncertainties. The matrices $\boldsymbol{B}_k$ and $\boldsymbol{D}_k$ are obtained by using the prior information of the practical systems.

The structure of the EKF [1]–[3] described by (1) and (2) is adopted for the design of the REKF

$$\hat{\boldsymbol{x}}_{k|k-1} = f(\hat{\boldsymbol{x}}_{k-1}) \tag{7}$$

$$\hat{\boldsymbol{x}}_k = \hat{\boldsymbol{x}}_{k|k-1} + \boldsymbol{K}_k \left[\boldsymbol{y}_k - h(\hat{\boldsymbol{x}}_{k|k-1})\right] \tag{8}$$

where $\hat{\boldsymbol{x}}_k \in R^l$ is the state estimate and $\boldsymbol{K}_k$ is the gain matrix to be determined. The estimation error and the corresponding covariance matrix are defined as

$$\widetilde{\boldsymbol{x}}_k = \boldsymbol{x}_k - \hat{\boldsymbol{x}}_k \tag{9}$$

$$\boldsymbol{\Sigma}_k = \mathrm{E}\left(\widetilde{\boldsymbol{x}}_k \widetilde{\boldsymbol{x}}_k^{\mathrm{T}}\right). \tag{10}$$

The objective of this correspondence paper is to design a filter with the structure described by (7) and (8), such that there exists a sequence of positive-definite matrices $\boldsymbol{P}_k$ $(0 \leq k \leq n)$ that satisfies

$$\boldsymbol{\Sigma}_k \leq \boldsymbol{P}_k. \tag{11}$$

The bound $\boldsymbol{P}_k$ is obtained by solving a Riccati difference equation (RDE) that is generalized to account for the presence of uncertainties. The filter parameter $\boldsymbol{K}_k$ is calculated using the RDE.

B. Error Covariance Matrix

In this section, we will give the formulation of the error covariance matrix $\boldsymbol{\Sigma}_k$. Define the prediction error and the corresponding covariance matrix as

$$\widetilde{\boldsymbol{x}}_{k|k-1} = \boldsymbol{x}_k - \hat{\boldsymbol{x}}_{k|k-1} \tag{12}$$

$$\boldsymbol{\Sigma}_{k|k-1} = \mathrm{E}\left(\widetilde{\boldsymbol{x}}_{k|k-1} \widetilde{\boldsymbol{x}}_{k|k-1}^{\mathrm{T}}\right). \tag{13}$$

Substituting (1) and (7) into (12), we have

$$\widetilde{\boldsymbol{x}}_{k|k-1} = f(\boldsymbol{x}_{k-1}) - f(\hat{\boldsymbol{x}}_{k-1}) + \boldsymbol{B}_k \eta_k \phi(\boldsymbol{x}_{k-1}) + \boldsymbol{w}_k. \tag{14}$$

Expanding $f(\boldsymbol{x}_{k-1})$ in a Taylor series about $\hat{\boldsymbol{x}}_{k-1}$ gives

$$f(\boldsymbol{x}_{k-1}) = f(\hat{\boldsymbol{x}}_{k-1}) + \boldsymbol{F}_k \widetilde{\boldsymbol{x}}_{k-1} + \Delta_f\left(\widetilde{\boldsymbol{x}}_{k-1}^2\right) \tag{15}$$

where $\boldsymbol{F}_k = \partial f(\boldsymbol{x})/\partial \boldsymbol{x}|_{\boldsymbol{x}=\hat{\boldsymbol{x}}_{k-1}}$ and $\Delta_f(\widetilde{\boldsymbol{x}}_{k-1}^2)$ represents the high-order terms of the Taylor series expansion. In order to facilitate the following deduction, the high-order terms are transformed into an equivalent formulation that is easy to handle:

$$\Delta_f\left(\widetilde{\boldsymbol{x}}_{k-1}^2\right) = \boldsymbol{A}_k \boldsymbol{\beta}_k \boldsymbol{L} \widetilde{\boldsymbol{x}}_{k-1} \tag{16}$$

where $\boldsymbol{A}_k \in R^{l\times l}$ is a problem-dependent scaling matrix and $\boldsymbol{\beta}_k \in R^{l\times l}$ is an unknown time-varying matrix introduced to take into account the linearization errors of the dynamics model. It is assumed that $\boldsymbol{\beta}_k$ is bounded, i.e.,

$$\boldsymbol{\beta}_k \boldsymbol{\beta}_k^{\mathrm{T}} \leq \boldsymbol{I}. \tag{17}$$

The matrix $\boldsymbol{L} \in \boldsymbol{R}^{l\times l}$ is introduced to provide an extra degree of freedom to tune the filter. In general, it can be set to identity matrix $\boldsymbol{I}$. From (15) and (16), (14) becomes

$$\widetilde{\boldsymbol{x}}_{k|k-1} = (\boldsymbol{F}_k + \boldsymbol{A}_k \boldsymbol{\beta}_k \boldsymbol{L})\widetilde{\boldsymbol{x}}_{k-1} + \boldsymbol{B}_k \eta_k \phi(\boldsymbol{x}_{k-1}) + \boldsymbol{w}_k. \tag{18}$$

Using (18) and (13), the covariance matrix of the prediction error is expressed as

$$\begin{aligned}\boldsymbol{\Sigma}_{k|k-1} = (\boldsymbol{F}_k + \boldsymbol{A}_k \boldsymbol{\beta}_k \boldsymbol{L})\boldsymbol{\Sigma}_{k-1}(\boldsymbol{F}_k + \boldsymbol{A}_k \boldsymbol{\beta}_k \boldsymbol{L})^{\mathrm{T}} \\ + q_k \boldsymbol{B}_k \mathrm{E}\left[\phi(\boldsymbol{x}_{k-1})\phi^{\mathrm{T}}(\boldsymbol{x}_{k-1})\right] \boldsymbol{B}_k^{\mathrm{T}} + \boldsymbol{Q}_k.\end{aligned} \tag{19}$$

Similarly, the estimation error in (9) can be written as

$$\widetilde{\boldsymbol{x}}_k = \widetilde{\boldsymbol{x}}_{k|k-1} - \boldsymbol{K}_k \left[(\boldsymbol{H}_k + \boldsymbol{C}_k \boldsymbol{\alpha}_k \boldsymbol{L})\widetilde{\boldsymbol{x}}_{k|k-1} + \boldsymbol{D}_k \boldsymbol{\xi}_k \psi(\boldsymbol{x}_k) + \boldsymbol{v}_k\right] \tag{20}$$

where $\boldsymbol{H}_k = \partial h(\boldsymbol{x})/\partial \boldsymbol{x}|_{\boldsymbol{x}=\hat{\boldsymbol{x}}_{k|k-1}}$, $\boldsymbol{C}_k \in R^{m\times l}$ is a problem-dependent scaling matrix, and $\boldsymbol{\alpha}_k \in R^{l\times l}$ is an unknown time-varying matrix to account for the linearization errors of the measurement model. It is assumed that

$$\boldsymbol{\alpha}_k \boldsymbol{\alpha}_k^{\mathrm{T}} \leq \boldsymbol{I}. \tag{21}$$

Substituting (20) into (10), we have

$$\begin{aligned}\boldsymbol{\Sigma}_k = &\left[\boldsymbol{I} - \boldsymbol{K}_k(\boldsymbol{H}_k + \boldsymbol{C}_k \boldsymbol{\alpha}_k \boldsymbol{L})\right] \boldsymbol{\Sigma}_{k|k-1} \\ &\times \left[\boldsymbol{I} - \boldsymbol{K}_k(\boldsymbol{H}_k + \boldsymbol{C}_k \boldsymbol{\alpha}_k \boldsymbol{L})\right]^{\mathrm{T}} \\ &+ \boldsymbol{K}_k \left\{r_k \boldsymbol{D}_k \mathrm{E}\left[\psi(\boldsymbol{x}_k)\psi^{\mathrm{T}}(\boldsymbol{x}_k)\right] \boldsymbol{D}_k^{\mathrm{T}} + \boldsymbol{R}_k\right\} \boldsymbol{K}_k^{\mathrm{T}}.\end{aligned} \tag{22}$$

So far, we have obtained the formulation of the error covariance matrix. However, as the parameters $\boldsymbol{\beta}_k$, q_k, $\boldsymbol{\alpha}_k$, and r_k are unknown, it is impossible to calculate the covariance matrix $\boldsymbol{\Sigma}_k$ from (19) and (22) directly. An alternative way is to find a set of upper bounds for $\boldsymbol{\Sigma}_k$ and then determine the filter gain $\boldsymbol{K}_k$ according to the upper bound.

C. REKF Design

The derivation of the filter is based on the following lemmas.

Lemma 1 [18]: Give matrices $\boldsymbol{A}$, $\boldsymbol{B}$, $\boldsymbol{C}$, and $\boldsymbol{D}$ with compatible dimensions such that $\boldsymbol{C}\boldsymbol{C}^{\mathrm{T}} \leq \boldsymbol{I}$. Let $\boldsymbol{U}$ be a symmetric positive-definite matrix and a be an arbitrary positive constant such that $a^{-1}\boldsymbol{I} - \boldsymbol{D}\boldsymbol{U}\boldsymbol{D}^{\mathrm{T}} > 0$; then, the following matrix inequality holds:

$$\begin{aligned}(\boldsymbol{A} + \boldsymbol{B}\boldsymbol{C}\boldsymbol{D})\boldsymbol{U}(\boldsymbol{A} + \boldsymbol{B}\boldsymbol{C}\boldsymbol{D})^{\mathrm{T}} \\ \leq \boldsymbol{A}(\boldsymbol{U}^{-1} - a\boldsymbol{D}^{\mathrm{T}}\boldsymbol{D})^{-1}\boldsymbol{A}^{\mathrm{T}} + a^{-1}\boldsymbol{B}\boldsymbol{B}^{\mathrm{T}}.\end{aligned} \tag{23}$$

Lemma 2 [19]: For $0 \leq k \leq n$, suppose that $\boldsymbol{U} = \boldsymbol{U}^{\mathrm{T}} > 0$, $e_k(\boldsymbol{U}) = e_k^{\mathrm{T}}(\boldsymbol{U}) \in R^{l\times l}$, and $g_k(\boldsymbol{U}) = g_k^{\mathrm{T}}(\boldsymbol{U}) \in R^{l\times l}$. If there exists $\boldsymbol{V} = \boldsymbol{V}^{\mathrm{T}} > \boldsymbol{U}$ such that

$$e_k(\boldsymbol{V}) \geq e_k(\boldsymbol{U}) \tag{24}$$

$$g_k(\boldsymbol{V}) \geq e_k(\boldsymbol{V}) \tag{25}$$

then the solutions $\boldsymbol{X}_k$ and $\boldsymbol{Y}_k$ to the following difference equations

$$\boldsymbol{X}_k = e_k(\boldsymbol{X}_{k-1}) \quad \boldsymbol{Y}_k = g_k(\boldsymbol{Y}_{k-1}) \quad \boldsymbol{X}_0 = \boldsymbol{Y}_0 > 0 \tag{26}$$

satisfy $\boldsymbol{X}_k \leq \boldsymbol{Y}_k$.

The main result of this correspondence paper is summarized in the following theorem.

Theorem 1: Consider the system described by (1) and (2). Assume that (17) and (21) are fulfilled. If there exists a positive constant γ, such that the following RDE

$$\boldsymbol{P}_0 = \boldsymbol{\Sigma}_0 \tag{27}$$

$$\boldsymbol{P}_{k|k-1} = \boldsymbol{F}_k \left(\boldsymbol{P}_{k-1}^{-1} - \gamma^{-2}\boldsymbol{L}^{\mathrm{T}}\boldsymbol{L}\right)^{-1} \boldsymbol{F}_k^{\mathrm{T}} + \gamma^2 \boldsymbol{A}_k \boldsymbol{A}_k^{\mathrm{T}} + \overline{\boldsymbol{Q}}_k \tag{28}$$

$$\begin{aligned}\boldsymbol{P}_k = (\boldsymbol{I} - \boldsymbol{K}_k \boldsymbol{H}_k)\left(\boldsymbol{P}_{k|k-1}^{-1} - \gamma^{-2}\boldsymbol{L}^{\mathrm{T}}\boldsymbol{L}\right)^{-1} (\boldsymbol{I} - \boldsymbol{K}_k \boldsymbol{H}_k)^{\mathrm{T}} \\ + \boldsymbol{K}_k \left(\gamma^2 \boldsymbol{C}_k \boldsymbol{C}_k^{\mathrm{T}} + \overline{\boldsymbol{R}}_k\right) \boldsymbol{K}_k^{\mathrm{T}}\end{aligned} \tag{29}$$

where

$$\overline{\boldsymbol{Q}}_k = \boldsymbol{B}_k \Xi_k \boldsymbol{B}_k^{\mathrm{T}} + \boldsymbol{Q}_k \quad \overline{\boldsymbol{R}}_k = \boldsymbol{D}_k \Theta_k \boldsymbol{D}_k^{\mathrm{T}} + \boldsymbol{R}_k \tag{30}$$

have positive-define solutions $\boldsymbol{P}_k$ and

$$\gamma^2\boldsymbol{I}-\boldsymbol{L}\boldsymbol{P}_k\boldsymbol{L}^{\mathrm{T}}>0\quad \gamma^2\boldsymbol{I}-\boldsymbol{L}\boldsymbol{P}_{k|k-1}\boldsymbol{L}^{\mathrm{T}}>0 \tag{31}$$

then the estimation error of the REKF shown in (7) and (8) with gain

$$\begin{aligned}\boldsymbol{K}_k=&\left(\boldsymbol{P}_{k|k-1}^{-1}-\gamma^{-2}\boldsymbol{L}^{\mathrm{T}}\boldsymbol{L}\right)^{-1}\boldsymbol{H}_k^{\mathrm{T}}\\ &\times\left[\boldsymbol{H}_k\left(\boldsymbol{P}_{k|k-1}^{-1}-\gamma^{-2}\boldsymbol{L}^{\mathrm{T}}\boldsymbol{L}\right)^{-1}\boldsymbol{H}_k^{\mathrm{T}}+\gamma^2\boldsymbol{C}_k\boldsymbol{C}_k^{\mathrm{T}}+\overline{\boldsymbol{R}}_k\right]^{-1}\end{aligned} \tag{32}$$

will satisfy the boundedness condition

$$\mathrm{E}\left(\widetilde{\boldsymbol{x}}_k\widetilde{\boldsymbol{x}}_k^{\mathrm{T}}\right)\le\boldsymbol{P}_k,\qquad 0\le k\le n. \tag{33}$$

Moreover, the REKF minimizes the bound $\boldsymbol{P}_k$.

The proof of *Theorem 1* is collected in the Appendix.

The tuning parameter γ, which has been used for the design of the H_∞ filter in [6] and [8], gives an upper bound of the energy gain from the uncertainties to the estimation errors. It is clarified in *Theorem 1* that, if the appropriate parameter γ is found such that $\boldsymbol{P}_k>0$, the estimation error of the REKF will remain bounded. Note that the parameter γ should be sufficiently large such that (31) is satisfied. For the sake of clarity, the REKF algorithm is summarized as follows:

Prediction. The one-step prediction and its corresponding error covariance matrix are obtained with (7) and (28).

Update. The estimate of state and the corresponding error covariance matrix are calculated with (8) and (29).

Remarks:

1) It can be seen from (7), (28), (8), and (29) that the REKF has the structure of the EKF. If the effects of the linearization errors and the model uncertainties are negligible, $\boldsymbol{A}_k$, $\boldsymbol{B}_k$, $\boldsymbol{C}_k$, and $\boldsymbol{D}_k$ should be set to zero. In addition, if the robust performance is not required, $\boldsymbol{L}$ could also be set to zero, and then the REKF will revert to the EKF.
2) There exist many free design parameters in the expression of the REKF. The matrices $\boldsymbol{A}_k$, $\boldsymbol{B}_k$, $\boldsymbol{C}_k$, and $\boldsymbol{D}_k$ are introduced to scale the linearization errors of the dynamic model, the uncertainties of the dynamic model, the linearization errors of the measurement model, and the uncertainties of the measurement model, respectively. This gives the possibility for taking different kinds of disturbances into account for the design of the filter gain $\boldsymbol{K}_k$ so that the dependence of the filter on the dynamic or observation model with the uncertainties will be weakened.

III. Analysis of REKF

In this section, we will derive an important characteristic of the proposed filter, i.e., the robust performance. An interpretation of the robust performance is that the energy ratio between the model uncertainties and the estimation error is bounded. We restrict our attention to systems with linear dynamic models. The performance of the REKF can be evaluated by the following theorem.

Theorem 2: Consider the following system:

$$\boldsymbol{x}_k=\boldsymbol{F}_k\boldsymbol{x}_{k-1}+\boldsymbol{B}_k\eta_k\phi(\boldsymbol{x}_{k-1})+\boldsymbol{w}_k \tag{34}$$

$$\boldsymbol{y}_k=h(\boldsymbol{x}_k)+\boldsymbol{D}_k\xi_k\psi(\boldsymbol{x}_k)+\boldsymbol{v}_k \tag{35}$$

where $\boldsymbol{F}_k\in R^{l\times l}$ is a known time-varying matrix, and the REKF is stated by (7), (8), (28), and (29). If (21) and (31) are fulfilled and the following assumptions hold for every $0\le k\le n$

$$\det\left[\boldsymbol{I}-\boldsymbol{K}_k(\boldsymbol{H}_k+\boldsymbol{C}_k\boldsymbol{\alpha}_k\boldsymbol{L})\right]\neq0\quad \det(\boldsymbol{F}_k)\neq0\quad \det(\boldsymbol{L})\neq0 \tag{36}$$

then

$$\frac{\sum_{k=0}^{n}\|\widetilde{\boldsymbol{x}}_k\|^2_{\boldsymbol{L}^{\mathrm{T}}\boldsymbol{L}}}{\|\widetilde{\boldsymbol{x}}_0\|^2_{\boldsymbol{P}_0^{-1}}+\sum_{k=1}^{n}\left(\|\overline{\boldsymbol{w}}_k\|^2_{\boldsymbol{Q}_k}+\|\overline{\boldsymbol{v}}_k\|^2_{\boldsymbol{R}_k}\right)}\le\gamma^2 \tag{37}$$

where $\overline{\boldsymbol{w}}_k=\boldsymbol{B}_k\eta_k\phi(\boldsymbol{x}_{k-1})+\boldsymbol{w}_k$, $\overline{\boldsymbol{v}}_k=\boldsymbol{D}_k\xi_k\psi(\boldsymbol{x}_k)+\boldsymbol{v}_k$, and the notation $\|\boldsymbol{x}\|^2_{\boldsymbol{P}}$ is defined as the mean of the square of the weighted (by $\boldsymbol{P}$) L_2 norm of $\boldsymbol{x}$, i.e., $\|\boldsymbol{x}\|^2_{\boldsymbol{P}}=\mathrm{E}(\boldsymbol{x}^{\mathrm{T}}\boldsymbol{P}\boldsymbol{x})$.

The proof of *Theorem 2* is collected in the Appendix.

Equation (37) shows that the proposed filter can guarantee robustness against system model uncertainties, as well as process and measurement noises. Equation (37) arises from the H_∞ design.

Remarks:

1) Although the parameter γ is valuable to facilitate the derivation and the interpretation of the filter, in practice, it may be difficult to improve the filter performance by tuning γ. See [20] for more explanations about this limitation.
2) For the system with nonlinear dynamic model and linear measurement model, the performance of the REKF can be analyzed in a similar way. The relevant derivation is omitted for the sake of simplicity.

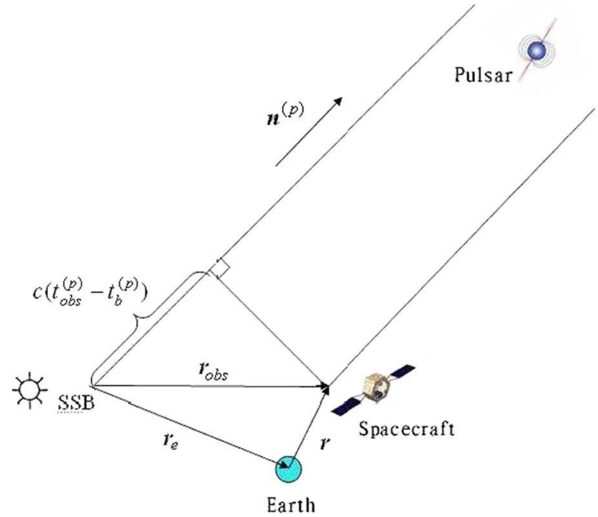

Fig. 1. Geometric relation between the position and the measurements.

IV. Simulation

A. System Model

The model of the X-ray pulsar positioning system is adopted here to illustrate the high performance of the proposed REKF. The state vector is chosen as $\boldsymbol{x}_k=[\boldsymbol{r}\quad\boldsymbol{v}]$, where $\boldsymbol{r}=[r_x\quad r_y\quad r_z]^{\mathrm{T}}$ is the spacecraft position vector and $\boldsymbol{v}=[v_x\quad v_y\quad v_z]^{\mathrm{T}}$ is the velocity vector. Using a Euler discretization of step size τ, the dynamic model is as follows:

$$f(\boldsymbol{x}_{k-1})=\boldsymbol{x}_{k-1}+\begin{bmatrix}v_x\\ v_y\\ v_z\\ -\mu r_x/r^3\\ -\mu r_y/r^3\\ -\mu r_z/r^3\end{bmatrix}\tau \tag{38}$$

TABLE I
LIST OF X-RAY PULSAR POSITION AND ATTRIBUTES

Name	Ecliptic longitude(°)	Ecliptic latitude(°)	Distance (*kpc*)[a]	Period (s)	FWHW[b] (s)	Flux (photons/cm^2/s)
B0531+21	84.10	-1.30	2.0 ± 0.5	0.0335	1.7×10^{-3}	10.34
B1821-24	275.57	-1.55	5.1 ± 0.5	0.00305	5.5×10^{-5}	0.00710
B1937+21	301.82	42.30	3.6 ± 0.5	0.00156	2.1×10^{-5}	0.00231

[a] 1kpc = 3×10^{19}m
[b] The 50% width of the pulse profile, or Full-Width Half-Maximum.

where the denotation μ is the gravitational constant of the celestial body and $r = (r_x^2 + r_y^2 + r_z^2)^{0.5}$. Note that the time dependence of the variables $\boldsymbol{r}$ and $\boldsymbol{v}$ is omitted for notational convenience. The model uncertainties in the dynamic model are considered to be negligible, i.e., $\boldsymbol{B}_k = 0$.

The measurement model of the pulsar positioning system is written as

$$t_{\text{obs}}^{(p)} = t_b^{(p)} - \frac{1}{c}\boldsymbol{n}^{(p)} \cdot \boldsymbol{r}_{\text{obs}} + \frac{1}{2cd^{(p)}}\left[r_{\text{obs}}^2 - \left(\boldsymbol{n}^{(p)} \cdot \boldsymbol{r}_{\text{obs}}\right)^2\right] - \frac{2\mu_s}{c^3}\ln\left|\boldsymbol{n}^{(p)} \cdot \boldsymbol{r}_{\text{obs}} + r_{\text{obs}}\right| + v_k^{(p)} \quad (39)$$

where the superscript (p) is used to distinguish different pulsars and $t_{\text{obs}}^{(p)}$ and $t_b^{(p)}$ denote the arrival time of a pulsar signal at the spacecraft and the arrival time of the same pulse at the solar system barycenter (SSB). $t_{\text{obs}}^{(p)}$ can be measured by the X-ray detector, and $t_b^{(p)}$ can be predicted precisely through a pulsar phase model. The denotation c is the speed of light, $\boldsymbol{n}^{(p)}$ is the unit position vector of the pth pulsar relative to the SSB, and $\boldsymbol{r}_{\text{obs}}$ is the position vector of the spacecraft relative to the SSB. The relation between $\boldsymbol{r}_{\text{obs}}$ and $\boldsymbol{r}$ is $\boldsymbol{r}_{\text{obs}} = \boldsymbol{r}_c + \boldsymbol{r}$, where $\boldsymbol{r}_c$ is the known position vector of the celestial body. $d^{(p)}$ is the distance between the pth pulsar and the SSB, which cannot be measured precisely at present. μ_s is the gravitational constant of the sun, and $v_k^{(p)}$ denotes the measurement noise. The relation between the time difference $t_{\text{obs}}^{(p)} - t_b^{(p)}$ and the position vector $\boldsymbol{r}_{\text{obs}}$ is shown roughly in Fig. 1.

Clearly, the difference between the predicted and measured pulse arrival times represents the position of the spacecraft relative to the SSB. However, the inaccurate model parameter $d^{(p)}$ may introduce a bias in the estimate. In the design of the REKF, the system errors caused by $d^{(p)}$ are treated as model uncertainties. The distance $d^{(p)}$ is assumed to be in the scope $[\hat{d}^{(p)} - \Delta d^{(p)} \quad \hat{d}^{(p)} + \Delta d^{(p)}]$, where $\hat{d}^{(p)}$ denotes the measured distance and $\Delta d^{(p)}$ is the bound of the parameter uncertainty. Based on this formulation, the observation model for the pth pulsar can be rewritten in the form of (2)

$$h^{(p)}(x_k) = t_b^{(p)} - \frac{1}{c}\boldsymbol{n}^{(p)} \cdot \boldsymbol{r}_{\text{obs}} + \frac{1}{2c\hat{d}^{(p)}}\left[r_{\text{obs}}^2 - \left(\boldsymbol{n}^{(p)} \cdot \boldsymbol{r}_{\text{obs}}\right)^2\right] - \frac{2\mu_s}{c^3}\ln\left|\boldsymbol{n}^{(p)} \cdot \boldsymbol{r}_{\text{obs}} + r_{\text{obs}}\right| \quad (40)$$

$$D_k^{(p)} = \kappa\left(\frac{1}{\hat{d}^{(p)} - \Delta d^{(p)}} - \frac{1}{\hat{d}^{(p)} + \Delta d^{(p)}}\right), \qquad \kappa > 1 \quad (41)$$

$$\psi^{(p)}(x_k) = \frac{1}{2c}\left[r_{\text{obs}}^2 - \left(\boldsymbol{n}^{(p)} \cdot \boldsymbol{r}_{\text{obs}}\right)^2\right]. \quad (42)$$

The role of the matrix $D^{(p)}$ is to scale the magnitude of the model uncertainty. Intuitively, when the parameter κ is chosen to be large enough, the assumption in (5) ($\mathrm{E}(\xi_k^2) = r_k, r_k \leq 1$) will be fulfilled. In this correspondence paper, κ is set to 50.

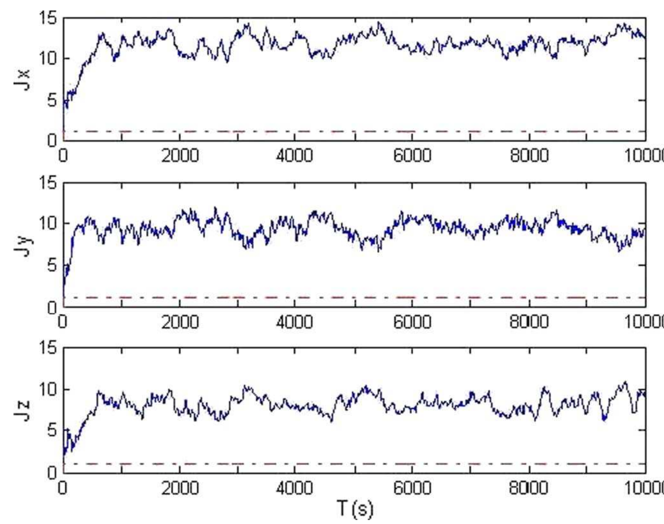

Fig. 2. Normalized estimation error of the EKF.

B. Simulation Results

The following three filtering algorithms are used for comparison: the standard EKF, the extended robust H_∞ filter proposed in [11], and the REKF described by (7), (8), (28), and (29). For the implementation of the REKF, the free parameters, i.e., γ, $\boldsymbol{L}$, $\boldsymbol{A}_k$, $\boldsymbol{C}_k$, $\overline{\boldsymbol{Q}}_k$, and $\overline{\boldsymbol{R}}_k$, should be chosen properly. To ensure that the conditions in (31) are fulfilled, the parameter γ is designed as

$$\gamma = 10\max\left(\mathrm{eig}(\boldsymbol{L}\boldsymbol{P}_0\boldsymbol{L}^{\mathrm{T}})\right)^{0.5} \quad (43)$$

where $\max(\mathrm{eig}(\boldsymbol{P}))$ indicates the maximum eigenvalue of the matrix $\boldsymbol{P}$. The parameter matrix $\boldsymbol{L}$ is simply set as $\boldsymbol{L} = \boldsymbol{I}$. The matrices $\boldsymbol{A}_k$ and $\boldsymbol{C}_k$ are introduced to scale the magnitude of the linearization errors. As the nonlinear terms in (38) and (40) are relatively small, the matrices are set to zero. The matrices $\overline{\boldsymbol{Q}}_k$ and $\overline{\boldsymbol{R}}_k$ are used to account for the model uncertainties. As $\boldsymbol{B}_k = 0$, we choose $\overline{\boldsymbol{Q}}_k = \boldsymbol{Q}_k$. According to (30) and (3), the matrix $\overline{\boldsymbol{R}}_k^{(p)}$ is designed as

$$\overline{\boldsymbol{R}}_k^{(p)} = \boldsymbol{D}_k^{(p)}\left[\psi^{(p)}(\hat{\boldsymbol{x}}_k)\right]^2\boldsymbol{D}_k^{(p)} + \boldsymbol{R}_k^{(p)}. \quad (44)$$

It is assumed that the spacecraft rotates around a satellite of Jupiter with the initial orbital elements: semimajor axis $a = 2700$ km, eccentricity $e = 0.0018$, inclination $i = 65°$, right ascending node $\Omega = 30°$, argument of perigee $\omega = 30°$, and mean anomaly $M = 0°$. The measurement noise covariance matrix is determined using the method in [15, eq. (4.100), pp. 4–7] according to the attributes of the pulsars shown in Table I

$$\boldsymbol{R}_k = \mathrm{diag}\left(\left(\sigma^{(1)}\right)^2 \quad \left(\sigma^{(2)}\right)^2 \quad \left(\sigma^{(3)}\right)^2\right) \quad (45)$$

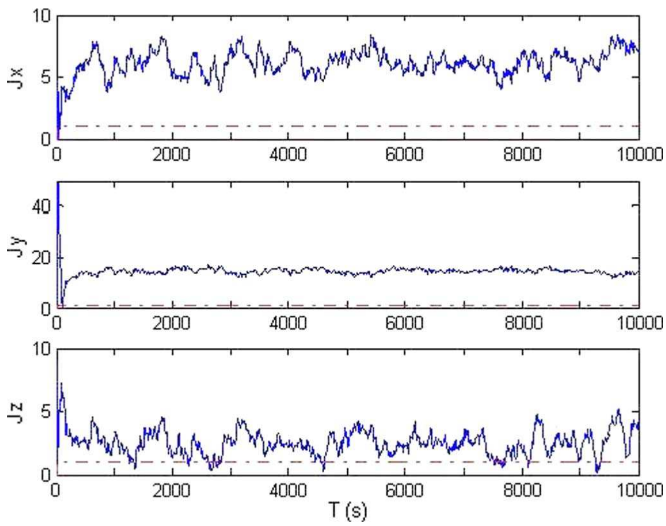

Fig. 3. Normalized estimation error of the extended robust H_∞ filter.

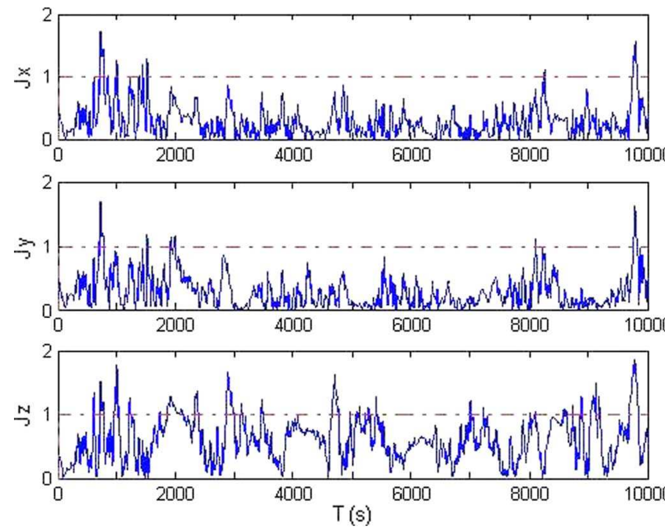

Fig. 4. Normalized estimation error of the REKF.

where $c\sigma^{(1)} = 25.1$ m, $c\sigma^{(2)} = 277.8$ m, and $c\sigma^{(3)} = 313.3$ m.

The normalized estimation errors, which can be calculated by

$$J_x = \sqrt{\widetilde{\boldsymbol{x}}_{k,1}^2 \boldsymbol{P}_k(1,1)^{-1}} \quad J_y = \sqrt{\widetilde{\boldsymbol{x}}_{k,2}^2 \boldsymbol{P}_k(2,2)^{-1}}$$

$$J_z = \sqrt{\widetilde{\boldsymbol{x}}_{k,3}^2 \boldsymbol{P}_k(3,3)^{-1}}$$

where $\widetilde{\boldsymbol{x}}_{k,i}$ is the ith element in the state vector $\widetilde{\boldsymbol{x}}_k$ and $\boldsymbol{P}_k(i,i)$ is the ith diagonal element of the matrix $\boldsymbol{P}_k$, are adopted to check the performance of the filters. The normalized estimation errors of the EKF are plotted versus k in Fig. 2. Clearly, the normalized estimation error is always larger than one (represented by broken lines). It indicates that the performance of the EKF for the considered system is rather poor. Model uncertainties lead to biased estimates and an overoptimistic error covariance matrix. Certainly, the performance of the EKF can be improved by artificially tuning the matrices $\boldsymbol{Q}_k$ and $\boldsymbol{R}_k$ of the algorithm. However, tuning is not an acceptable part of the Kalman theoretical framework.

The normalized estimation errors of the extended robust H_∞ filter are shown in Fig. 3. As expected, the effect of the uncertainties in the measurement model is partly eliminated by tuning a certain parameter in the algorithm. However, evident deviations still remain in the estimation results. Moreover, the error covariance matrix of the algorithm is still overoptimistic. As the model uncertainties caused by inaccurate $\hat{d}^{(p)}$ are different for the observations from different pulsars, it is difficult to fully compensate them by tuning the filtering parameters manually in this scenario.

Fig. 4 shows the estimation results of the REKF. As we expected, the estimate of the REKF is more accurate than that of the EKF, and the filter is consistent at most times. The algorithm is less sensitive to the model uncertainties in that the effect of the uncertainties to the state estimate is suppressed and the information without uncertainties or with minor uncertainties is utilized adequately. In addition, it is worth mentioning that the free parameters of the REKF have an explicit physical explanation.

Furthermore, the root-mean-square (rms) errors of the three algorithms are calculated from ten independent trials and shown together in Fig. 5, where the abbreviation ERHF denotes the extended robust H_∞ filter. The Cramer–Rao lower bound (CRLB), which provides a theoretical lower bound on the rms error of a state estimate, is calculated according to the method in [21]. As the CRLB is derived with

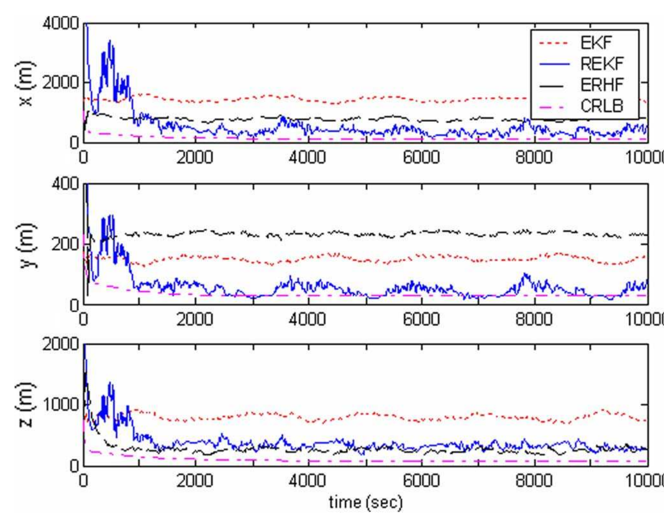

Fig. 5. RMS errors of the EKF, the extended robust H_∞ filter, and the REKF.

the assumption that the process noise is zero-mean white Gaussian noise, the CRLB values shown in Fig. 5 are heuristic. The means of the rms errors for $k = 1 : 10\,000$ and the norm of the means are listed in Table II. From Fig. 5 and Table II, it is fair to say that the proposed method outperforms the standard EKF and the extended robust H_∞ filter for the considered system. As the difference of the time expense between the REKF and the EKF is negligible, we indicate that the computation loads of the two algorithms are roughly the same.

V. Conclusion

An REKF is designed for nonlinear uncertain systems, which guarantees an upper bound on the estimation error. Further analysis shows that the proposed filter guarantees a bounded energy gain from the model uncertainties to the estimation errors. The REKF is easy to implement in practice, as few parameters have to be tuned for the design of the filter and no additional computation is required. The simulation results show that the unfavorable effects of the model uncertainties are reduced efficiently by using the REKF for the X-ray pulsar positioning system.

TABLE II
ESTIMATION ERRORS OF THE THREE ALGORITHMS

Algorithm	position errors (m)				velocity errors (m/s)			
	r_x	r_y	r_z	norm	v_x	v_y	v_z	norm
EKF	1442.9	149.9	791.5	1652.5	0.8929	0.2133	0.6322	1.115
extended robust H_∞ filter	775.4	238.2	274.2	856.3	0.5889	0.1790	0.4540	0.7648
REKF	578.7	62.5	382.1	696.3	0.5364	0.1804	0.4330	0.7126

APPENDIX

A. Proof of Theorem 1

Proof: From (19) and (22), it is easy to see that, if the covariance matrix $\boldsymbol{\Sigma}_{k-1}^{(2)} \geq \boldsymbol{\Sigma}_{k-1}^{(1)}$ (the superscript is used to distinguish different covariance matrices), then the following inequalities fulfill:

$$\boldsymbol{\Sigma}_{k|k-1}\left(\boldsymbol{\Sigma}_{k-1}^{(2)}\right) \geq \boldsymbol{\Sigma}_{k|k-1}\left(\boldsymbol{\Sigma}_{k-1}^{(1)}\right) \quad \text{(A1)}$$

$$\boldsymbol{\Sigma}_{k}\left(\boldsymbol{\Sigma}_{k|k-1}\left(\boldsymbol{\Sigma}_{k-1}^{(2)}\right)\right) \geq \boldsymbol{\Sigma}_{k}\left(\boldsymbol{\Sigma}_{k|k-1}\left(\boldsymbol{\Sigma}_{k-1}^{(1)}\right)\right). \quad \text{(A2)}$$

In (A1) and (A2), $\boldsymbol{\Sigma}_{k|k-1}$ and $\boldsymbol{\Sigma}_k$ are written as the functions of $\boldsymbol{\Sigma}_{k-1}$ and $\boldsymbol{\Sigma}_{k|k-1}$, respectively. Substituting (32) into (29) and applying the matrix inversion lemma (see, e.g., [22, Appendix A2, p. 347]) yield

$$\boldsymbol{P}_k(\boldsymbol{P}_{k|k-1}) = \left[\boldsymbol{P}_{k|k-1}^{-1} - \gamma^{-2}\boldsymbol{L}^{\mathrm{T}}\boldsymbol{L} + \boldsymbol{H}_k^{\mathrm{T}}\left(\gamma^2\boldsymbol{C}_k\boldsymbol{C}_k^{\mathrm{T}} + \boldsymbol{D}_k\Theta_k\boldsymbol{D}_k^{\mathrm{T}} + \boldsymbol{R}_k\right)\boldsymbol{H}_k\right]^{-1}. \quad \text{(A3)}$$

It is easy to see from (A3) that, if $\boldsymbol{P}_{k|k-1}^{(2)} \geq \boldsymbol{P}_{k|k-1}^{(1)}$, then

$$\boldsymbol{P}_k\left(\boldsymbol{P}_{k|k-1}^{(2)}\right) \geq \boldsymbol{P}_k\left(\boldsymbol{P}_{k|k-1}^{(1)}\right). \quad \text{(A4)}$$

According to *Lemma 1* and (3), (6), (17), and (31), we have

$$\boldsymbol{P}_{k|k-1}(\boldsymbol{P}_{k-1}) \geq \boldsymbol{\Sigma}_{k|k-1}(\boldsymbol{P}_{k-1}). \quad \text{(A5)}$$

From (A4), we obtain

$$\boldsymbol{P}_k\left(\boldsymbol{P}_{k|k-1}(\boldsymbol{P}_{k-1})\right) \geq \boldsymbol{P}_k\left(\boldsymbol{\Sigma}_{k|k-1}(\boldsymbol{P}_{k-1})\right). \quad \text{(A6)}$$

According to *Lemma 1* and (3), (6), (21), and (31), we have

$$\boldsymbol{P}_k\left(\boldsymbol{\Sigma}_{k|k-1}(\boldsymbol{P}_{k-1})\right) \geq \boldsymbol{\Sigma}_k\left(\boldsymbol{\Sigma}_{k|k-1}(\boldsymbol{P}_{k-1})\right). \quad \text{(A7)}$$

From (A6) and (A7), the following inequality is obtained:

$$\boldsymbol{P}_k\left(\boldsymbol{P}_{k|k-1}(\boldsymbol{P}_{k-1})\right) \geq \boldsymbol{\Sigma}_k\left(\boldsymbol{\Sigma}_{k|k-1}(\boldsymbol{P}_{k-1})\right). \quad \text{(A8)}$$

Considering (A2) and (A8) and applying *Lemma 2*, we can draw a conclusion that

$$\boldsymbol{\Sigma}_k \leq \boldsymbol{P}_k, \qquad 0 \leq k \leq N. \quad \text{(A9)}$$

Then, take the partial derivatives of $\boldsymbol{P}_k$ with respect to $\boldsymbol{K}_k$ as follows:

$$\frac{\partial \boldsymbol{P}_k}{\partial \boldsymbol{K}_k} = 2(\boldsymbol{I} - \boldsymbol{K}_k\boldsymbol{H}_k)\left(\boldsymbol{P}_{k|k-1}^{-1} - \gamma^{-2}\boldsymbol{L}^{\mathrm{T}}\boldsymbol{L}\right)\left(-\boldsymbol{H}_k^{\mathrm{T}}\right) + 2\boldsymbol{K}_k\left(\gamma^2\boldsymbol{C}_k\boldsymbol{C}_k^{\mathrm{T}} + \boldsymbol{D}_k\Theta_k\boldsymbol{D}_k^{\mathrm{T}} + \boldsymbol{R}_k\right). \quad \text{(A10)}$$

Let $\partial \boldsymbol{P}_k / \partial \boldsymbol{K}_k = 0$; through straightforward algebraic manipulation, we obtain the optimal filter gain, as shown in (32), and this completes the proof of *Theorem 1*. □

B. Proof of Theorem 2

Proof: Substituting (18) into (20) and considering that, for the system described by (34) and (35), $\boldsymbol{A}_k = 0$, we have

$$\widetilde{\boldsymbol{x}}_k = [\boldsymbol{I} - \boldsymbol{K}_k(\boldsymbol{H}_k + \boldsymbol{C}_k\boldsymbol{\alpha}_k\boldsymbol{L})]\,\boldsymbol{F}_k\widetilde{\boldsymbol{x}}_{k-1} + [\boldsymbol{I} - \boldsymbol{K}_k(\boldsymbol{H}_k + \boldsymbol{C}_k\boldsymbol{\alpha}_k\boldsymbol{L})]\,\overline{\boldsymbol{w}}_k - \boldsymbol{K}_k\overline{\boldsymbol{v}}_k. \quad \text{(A11)}$$

Hence, the following equation is obtained:

$$\begin{aligned}\|\widetilde{\boldsymbol{x}}_k\|^2_{\boldsymbol{P}_k^{-1}} &= \mathrm{E}\left(\widetilde{\boldsymbol{x}}_k^{\mathrm{T}}\boldsymbol{P}_k^{-1}\widetilde{\boldsymbol{x}}_k\right)\\ &= \mathrm{E}\Big\{\widetilde{\boldsymbol{x}}_{k-1}^{\mathrm{T}}\boldsymbol{F}_k^{\mathrm{T}}\left[\boldsymbol{I} - \boldsymbol{K}_k(\boldsymbol{H}_k + \boldsymbol{C}_k\boldsymbol{\alpha}_k\boldsymbol{L})\right]^{\mathrm{T}}\boldsymbol{P}_k^{-1}\\ &\quad \times [\boldsymbol{I} - \boldsymbol{K}_k(\boldsymbol{H}_k + \boldsymbol{C}_k\boldsymbol{\alpha}_k\boldsymbol{L})]\,\boldsymbol{F}_k\widetilde{\boldsymbol{x}}_{k-1}\\ &\quad + \overline{\boldsymbol{w}}_k^{\mathrm{T}}\left[\boldsymbol{I} - \boldsymbol{K}_k(\boldsymbol{H}_k + \boldsymbol{C}_k\boldsymbol{\alpha}_k\boldsymbol{L})\right]^{\mathrm{T}}\boldsymbol{P}_k^{-1}\\ &\quad \times [\boldsymbol{I} - \boldsymbol{K}_k(\boldsymbol{H}_k + \boldsymbol{C}_k\boldsymbol{\alpha}_k\boldsymbol{L})]\,\overline{\boldsymbol{w}}_k\\ &\quad + \overline{\boldsymbol{v}}_k^{\mathrm{T}}\boldsymbol{K}_k^{\mathrm{T}}\boldsymbol{P}_k^{-1}\boldsymbol{K}_k\overline{\boldsymbol{v}}_k\Big\}. \end{aligned} \quad \text{(A12)}$$

From (21), (31), and (29), applying *Lemma 1*, we get the following inequality:

$$\boldsymbol{P}_k \geq [\boldsymbol{I} - \boldsymbol{K}_k(\boldsymbol{H}_k + \boldsymbol{C}_k\boldsymbol{\alpha}_k\boldsymbol{L})]\,\boldsymbol{P}_{k|k-1} \times [\boldsymbol{I} - \boldsymbol{K}_k(\boldsymbol{H}_k + \boldsymbol{C}_k\boldsymbol{\alpha}_k\boldsymbol{L})]^{\mathrm{T}}. \quad \text{(A13)}$$

Using (A13), the second term in (A12) becomes

$$\overline{\boldsymbol{w}}_k^{\mathrm{T}}[\boldsymbol{I} - \boldsymbol{K}_k(\boldsymbol{H}_k + \boldsymbol{C}_k\boldsymbol{\alpha}_k\boldsymbol{L})]^{\mathrm{T}}\boldsymbol{P}_k^{-1}[\boldsymbol{I} - \boldsymbol{K}_k(\boldsymbol{H}_k + \boldsymbol{C}_k\boldsymbol{\alpha}_k\boldsymbol{L})]\,\overline{\boldsymbol{w}}_k \leq \overline{\boldsymbol{w}}_k^{\mathrm{T}}\boldsymbol{P}_{k|k-1}^{-1}\overline{\boldsymbol{w}}_k. \quad \text{(A14)}$$

Substituting (28) into (A14) yields

$$\overline{\boldsymbol{w}}_k^{\mathrm{T}}[\boldsymbol{I} - \boldsymbol{K}_k(\boldsymbol{H}_k + \boldsymbol{C}_k\boldsymbol{\alpha}_k\boldsymbol{L})]^{\mathrm{T}}\boldsymbol{P}_k^{-1}[\boldsymbol{I} - \boldsymbol{K}_k(\boldsymbol{H}_k + \boldsymbol{C}_k\boldsymbol{\alpha}_k\boldsymbol{L})]\,\overline{\boldsymbol{w}}_k \leq \overline{\boldsymbol{w}}_k^{\mathrm{T}}\overline{\boldsymbol{Q}}_k^{-1}\overline{\boldsymbol{w}}_k. \quad \text{(A15)}$$

From (29) and (32), it is easy to verify that

$$\boldsymbol{K}_k = \boldsymbol{P}_k\boldsymbol{H}_k^{\mathrm{T}}\left(\gamma^2\boldsymbol{C}_k\boldsymbol{C}_k^{\mathrm{T}} + \overline{\boldsymbol{R}}_k\right)^{-1}. \quad \text{(A16)}$$

Using (A16), the third term in (A12) becomes

$$\overline{\boldsymbol{v}}_k^{\mathrm{T}}\boldsymbol{K}_k^{\mathrm{T}}\boldsymbol{P}_k^{-1}\boldsymbol{K}_k\overline{\boldsymbol{v}}_k = \overline{\boldsymbol{v}}_k^{\mathrm{T}}\left(\gamma^2\boldsymbol{C}_k\boldsymbol{C}_k^{\mathrm{T}} + \overline{\boldsymbol{R}}_k\right)^{-1}\boldsymbol{H}_k\boldsymbol{P}_k\boldsymbol{H}_k^{\mathrm{T}} \times \left(\gamma^2\boldsymbol{C}_k\boldsymbol{C}_k^{\mathrm{T}} + \overline{\boldsymbol{R}}_k\right)^{-1}\overline{\boldsymbol{v}}_k. \quad \text{(A17)}$$

In addition, it can be verified that

$$\left(\gamma^2 \boldsymbol{C}_k \boldsymbol{C}_k^T + \overline{\boldsymbol{R}}_k\right)^{-1} - \left(\gamma^2 \boldsymbol{C}_k \boldsymbol{C}_k^T + \overline{\boldsymbol{R}}_k\right)^{-1} \times \boldsymbol{H}_k \boldsymbol{P}_k \boldsymbol{H}_k^T \left(\gamma^2 \boldsymbol{C}_k \boldsymbol{C}_k^T + \overline{\boldsymbol{R}}_k\right)^{-1} = \left[\boldsymbol{H}_k (\boldsymbol{P}_{k\,|\,k-1}^{-1} - \gamma^{-2} \boldsymbol{L}^T \boldsymbol{L})^{-1} \boldsymbol{H}_k^T + \gamma^2 \boldsymbol{C}_k \boldsymbol{C}_k^T + \overline{\boldsymbol{R}}_k\right]^{-1} \geq 0. \tag{A18}$$

Hence, the following inequality can be obtained:

$$\overline{\boldsymbol{v}}_k^{\mathrm{T}} \boldsymbol{K}_k^{\mathrm{T}} \boldsymbol{P}_k^{-1} \boldsymbol{K}_k \overline{\boldsymbol{v}}_k \leq \overline{\boldsymbol{v}}_k^{\mathrm{T}} \overline{\boldsymbol{R}}_k^{-1} \overline{\boldsymbol{v}}_k. \tag{A19}$$

From (A13), the first term in (A12) can be written as

$$\widetilde{\boldsymbol{x}}_{k-1}^T \boldsymbol{F}_k^T \left[\boldsymbol{I} - \boldsymbol{K}_k(\boldsymbol{H}_k + \boldsymbol{C}_k \boldsymbol{\alpha}_k \boldsymbol{L})\right]^T \boldsymbol{P}_k^{-1} [\boldsymbol{I} - \boldsymbol{K}_k(\boldsymbol{H}_k + \boldsymbol{C}_k \boldsymbol{\alpha}_k \boldsymbol{L})] \boldsymbol{F}_k \widetilde{\boldsymbol{x}}_{k-1} \leq \widetilde{\boldsymbol{x}}_{k-1}^T \boldsymbol{F}_k^T \boldsymbol{P}_{k\,|\,k-1}^{-1} \boldsymbol{F}_k \widetilde{\boldsymbol{x}}_{k-1}. \tag{A20}$$

Substituting (28) into (A20) yields

$$\widetilde{\boldsymbol{x}}_{k-1}^T \boldsymbol{F}_k^T \left[\boldsymbol{I} - \boldsymbol{K}_k(\boldsymbol{H}_k + \boldsymbol{C}_k \boldsymbol{\alpha}_k \boldsymbol{L})\right]^T \boldsymbol{P}_k^{-1} \times \left[\boldsymbol{I} - \boldsymbol{K}_k(\boldsymbol{H}_k + \boldsymbol{C}_k \boldsymbol{\alpha}_k \boldsymbol{L})\right] \boldsymbol{F}_k \widetilde{\boldsymbol{x}}_{k-1} \leq \widetilde{\boldsymbol{x}}_{k-1}^T \boldsymbol{P}_{k-1}^{-1} \widetilde{\boldsymbol{x}}_{k-1} - \gamma^{-2} \widetilde{\boldsymbol{x}}_{k-1}^T \boldsymbol{L}^T \boldsymbol{L} \tilde{x}_{k-1}. \tag{A21}$$

Considering (A15), (A19), and (A21), (A12) is modified as

$$\|\widetilde{\boldsymbol{x}}_k\|^2_{\boldsymbol{P}_k^{-1}} \leq \|\widetilde{\boldsymbol{x}}_{k-1}\|^2_{\boldsymbol{P}_{k-1}^{-1}} - \gamma^{-2} \|\widetilde{\boldsymbol{x}}_{k-1}\|^2_{\boldsymbol{L}^{\mathrm{T}}\boldsymbol{L}} + \|\overline{\boldsymbol{w}}_k\|^2_{\overline{\boldsymbol{Q}}_k^{-1}} + \|\overline{\boldsymbol{v}}_k\|^2_{\overline{\boldsymbol{R}}_k^{-1}}. \tag{A22}$$

By adding up both sides of (A22), we establish that

$$\|\widetilde{\boldsymbol{x}}_n\|^2_{\boldsymbol{P}_n^{-1}} \leq \|\widetilde{\boldsymbol{x}}_0\|^2_{\boldsymbol{P}_0^{-1}} - \gamma^{-2} \sum_{k=0}^{n-1} \|\widetilde{\boldsymbol{x}}_k\|^2_{\boldsymbol{L}^T\boldsymbol{L}} + \sum_{k=1}^{n} \left(\|\overline{\boldsymbol{w}}_k\|^2_{\overline{\boldsymbol{Q}}_k^{-1}} + \|\overline{\boldsymbol{v}}_k\|^2_{\overline{\boldsymbol{R}}_k^{-1}}\right). \tag{A23}$$

According to (31), we have

$$\boldsymbol{P}_n^{-1} > \gamma^{-2} \boldsymbol{L}^{\mathrm{T}} \boldsymbol{L}. \tag{A24}$$

Finally, from (A23) and (A24), the robust performance of the proposed filter is expressed as

$$\sum_{k=0}^{n} \|\widetilde{\boldsymbol{x}}_k\|^2_{\boldsymbol{L}^{\mathrm{T}}\boldsymbol{L}} \leq \gamma^2 \left[\|\widetilde{\boldsymbol{x}}_0\|^2_{\boldsymbol{P}_0^{-1}} + \sum_{k=1}^{n} \left(\|\overline{\boldsymbol{w}}_k\|^2_{\overline{\boldsymbol{Q}}_k^{-1}} + \|\overline{\boldsymbol{v}}_k\|^2_{\overline{\boldsymbol{R}}_k^{-1}}\right)\right]. \tag{A25}$$

This completes the proof of Theorem 2. □

REFERENCES

[1] S. Bolognani, L. Tubiana, and M. Zigliotto, "EKF-based sensorless IPM synchronous motor drive for flux-weakening applications," *IEEE Trans. Ind. Appl.*, vol. 39, no. 3, pp. 768–775, May/Jun. 2003.

[2] S. Wu, L. Hong, and J. R. Layne, "2D rigid-body target modeling for tracking and identification with GMTI/HRR measurements," *Proc. Inst. Elect. Eng.—Control Theory Appl.*, vol. 151, no. 4, pp. 429–438, Jul. 2004.

[3] H. Zhao and R. Shibasaki, "A novel system for tracking pedestrians using multiple single-row laser-range scanners," *IEEE Trans. Syst., Man, Cybern. A, Syst., Humans*, vol. 35, no. 2, pp. 283–291, Mar. 2005.

[4] G. C. Goodwin and K. S. Sin, *Adaptive Filtering Prediction and Control*. Englewood Cliffs, NJ: Prentice-Hall, 1984.

[5] Z. Wang and X. Liu, "On designing H_∞ filters with circular pole and error variance constraints," *IEEE Trans. Circuits Syst. II, Analog Digit. Signal Process.*, vol. 50, no. 3, pp. 139–143, Mar. 2003.

[6] G. A. Einicke and L. B. White, "Robust extended Kalman filtering," *IEEE Trans. Signal Process.*, vol. 47, no. 9, pp. 2596–2599, Sep. 1999.

[7] O. I. Kosmidou and Y. S. Boutalis, "A linear matrix inequality approach for guaranteed cost control of systems with state and input delays," *IEEE Trans. Syst., Man, Cybern. A, Syst., Humans*, vol. 36, no. 5, pp. 936–942, Sep. 2006.

[8] F. Yang, Z. Wang, and Y. S. Hung, "Robust Kalman filtering for discrete time-varying uncertain systems with multiplicative noises," *IEEE Trans. Autom. Control*, vol. 47, no. 7, pp. 1179–1183, Jul. 2002.

[9] J. Y. Ishihara, M. H. Terra, and J. C. T. Campos, "Robust Kalman filter for descriptor systems," *IEEE Trans. Autom. Control*, vol. 51, no. 8, pp. 1354–1358, Aug. 2006.

[10] W. Zhang, B. S. Chen, and C. S. Tseng, "Robust H_∞ filtering for nonlinear stochastic systems," *IEEE Trans. Signal Process.*, vol. 53, no. 2, pp. 589–598, Feb. 2005.

[11] J. Seo, M. J. Yu, C. G. Park, and J. G. Lee, "An extended robust H_∞ filter for nonlinear constrained uncertain systems," *IEEE Trans. Signal Process.*, vol. 54, no. 11, pp. 4471–4475, Nov. 2006.

[12] H. Gao and C. Wang, "Delay-dependent robust H_∞ and L_2– L_∞ filtering for a class of uncertain nonlinear time-delay systems," *IEEE Trans. Autom. Control*, vol. 48, no. 9, pp. 1661–1666, Sep. 2003.

[13] M. R. James and I. R. Petersen, "Nonlinear state estimation for uncertain systems with an integral constraint," *IEEE Trans. Signal Process.*, vol. 46, no. 11, pp. 2926–2937, Nov. 1998.

[14] S. I. Sheikh, D. J. Pines, K. S. Wood, P. S. Ray, M. N. Lovellette, and M. T. Wolff, "Spacecraft navigation using X-ray pulsars," *J. Guid. Control Dyn.*, vol. 29, no. 1, pp. 49–63, 2006.

[15] D. W. Woodfork, "The use of X-ray pulsars for aiding GPS satellite orbit determination," M.S. thesis, Air Force Inst. Technol., Wright-Patterson AFB, OH, 2005.

[16] K. S. Wood, M. Kowalski, M. N. Lovellette, P. S. Ray, M. T. Wolff, D. J. Yentis, R. M. Bandyopadhyay, G. Fewtrell, and P. L. Hertz, "The unconventional stellar aspect (USA) experiment on ARGOS," presented at the Amer. Inst. Aeronautics Astronautics (AIAA) Space Conf. Expo., Albuquerque, NM, 2001, AIAA Paper 2001-4664.

[17] K. Xiong, C. L. Wei, and L. D. Liu, "The use of X-ray pulsars for aiding navigation of satellites in constellations," *Acta Astronaut.*, vol. 64, no. 4, pp. 427–436, Feb. 2009.

[18] L. Xie, Y. C. Soh, and C. E. de Souza, "Robust Kalman filtering for uncertain discrete-time systems," *IEEE Trans. Autom. Control*, vol. 39, no. 6, pp. 1310–1314, Jun. 1994.

[19] Y. Theodor and U. Shaked, "Robust discrete-time minimum-variance filtering," *IEEE Trans. Signal Process.*, vol. 44, no. 2, pp. 181–189, Feb. 1996.

[20] K. Xiong, H. Y. Zhang, and L. D. Liu, "Adaptive robust extended Kalman filter for nonlinear stochastic systems," *IET Control Theory Appl.*, vol. 2, no. 3, pp. 239–250, Mar. 2008.

[21] M. Simandl, J. Kralovec, and P. Tichavsky, "Filtering, predictive, and smoothing Cramer–Rao bounds for discrete-time nonlinear dynamic systems," *Automatica*, vol. 37, no. 11, pp. 1703–1716, Nov. 2001.

[22] F. L. Levis, *Optimal Estimation*. New York: Wiley, 1986.